J Physiol 588.15 (2010) pp 2945–2960

In vivo expression of G-protein $\beta_1\gamma_2$ dimer in adult mouse skeletal muscle alters L-type calcium current and excitation–contraction coupling

Norbert Weiss[1], Claude Legrand[1], Sandrine Pouvreau[1], Hicham Bichraoui[3], Bruno Allard[1], Gerald W. Zamponi[2], Michel De Waard[3] and Vincent Jacquemond[1]

[1] *Integrative Cellular and Molecular Physiology, University of Lyon 1, UMR CNRS 5123, Villeurbanne, France*
[2] *Department of Physiology and Pharmacology, Hotchkiss Brain Institute, University of Calgary, Calgary, Canada*
[3] *Ion Channels, Functions and Pathologies, Grenoble Institute of Neurosciences, Inserm U836, Grenoble, France*

A number of G-protein-coupled receptors are expressed in skeletal muscle but their roles in muscle physiology and downstream effector systems remain poorly investigated. Here we explored the functional importance of the G-protein $\beta\gamma$ (G$\beta\gamma$) signalling pathway on voltage-controlled Ca^{2+} homeostasis in single isolated adult skeletal muscle fibres. A GFP-tagged G$\beta_1\gamma_2$ dimer was expressed *in vivo* in mice muscle fibres. The GFP fluorescence pattern was consistent with a G$\beta_1\gamma_2$ dimer localization in the transverse-tubule membrane. Membrane current and indo-1 fluorescence measurements performed under voltage-clamp conditions reveal a drastic reduction of both L-type Ca^{2+} current density and of peak amplitude of the voltage-activated Ca^{2+} transient in G$\beta_1\gamma_2$-expressing fibres. These effects were not observed upon expression of G$\beta_2\gamma_2$, G$\beta_3\gamma_2$ or G$\beta_4\gamma_2$. Our data suggest that the G-protein $\beta_1\gamma_2$ dimer may play an important regulatory role in skeletal muscle excitation–contraction coupling.

(Resubmitted 15 April 2010; accepted after revision 11 June 2010; first published online 14 June 2010)
Corresponding author N. Weiss: Université Lyon 1 – UMR CNRS 5123 – Physiologie Intégrative Cellulaire et Moléculaire; Bât. R. Dubois; 43 boulevard du 11 novembre 1918, 69622 Villeurbanne, France. Email: norbert.weiss@yahoo.fr

Abbreviations FDB, flexor digitorum brevis; GPCR, G-protein-coupled receptor; DHPR, dihydropyridine receptor; RyR, ryanodine receptor; SR, sarcoplasmic reticulum.

Introduction

G-protein-coupled receptors (GPCRs) represent a large family of cell plasma membrane receptors that are involved in the transduction of extracellular signals into cellular responses (for review see Milligan & Kostenis, 2006). Activation of GPCRs following extracellular agonist stimulation results in the activation of two intracellular signalling molecules, Gα-GTP and the free G$\beta\gamma$ dimer. Whereas Gα-dependent signalling pathways involve the activation of soluble messenger cascades such as adenylyl cyclases, cyclic GMP phosphodiesterases or phospholipases Cβ, G$\beta\gamma$-mediated regulation generally occurs through direct binding of the dimer to target effectors. One such class of targeted receptors is represented by voltage-gated calcium channels (for review see McCudden *et al.* 2005).

In skeletal muscle, no less than 43 GPCRs were found to be expressed at the protein or mRNA level. Signalling activity of these GPCRs is suspected to play a role in the regulation of several aspects of muscle physiology, including plasticity, differentiation, pain, but also more specifically in the control of glucose uptake and of ion transport and membrane excitability (for review see Jean-Baptiste *et al.* 2005). Early sets of data also suggested that G-proteins may be involved in the regulation of the excitation–contraction (E–C) coupling process. In skeletal muscle, E–C coupling relies on a tight control of sarcoplasmic reticulum (SR) Ca^{2+} release through the type 1 ryanodine receptor (RyR1) by the voltage-sensing dihydropyridine receptor (DHPR)/$Ca_v1.1$ Ca^{2+} channel. Activation of the $Ca_v1.1$ subunit in response to transverse (T-) tubule membrane depolarization directly activates RyR1, allowing rapid mobilization of the SR Ca^{2+} store and the rise in myoplasmic Ca^{2+} concentration that triggers contraction (for review see Dulhunty, 2006). A possible functional role of GPCR signalling in the regulation of E–C coupling was suggested by experiments in skinned skeletal muscle fibres in which it was shown that constitutive activation of G-proteins by GTPγS either enhanced calcium- or caffeine-induced calcium release (Villaz *et al.* 1989) or directly elicited fibre contraction (Di Virgilio *et al.*

DOI: 10.1113/jphysiol.2010.191593

1986; Somasundaram *et al.* 1991). Furthermore, GTPγS was also reported to increase DHPR L-type Ca^{2+} current and intramembrane charge movement measured under vaseline-gap voltage-clamp conditions in rat and frog cut skeletal muscle fibres (Garcia *et al.* 1990). However, the issue became controversial as Lamb & Stephenson (1991) found no effect of GTPγS on both depolarization-induced Ca^{2+} release in skinned rat fibres and on intramembrane charge movement in rat cut fibres. Differences in the experimental conditions between these studies are most probably responsible for these discrepancies. Nevertheless, the use of GTPγS under such conditions remains a rather limited approach. First, in both skinned and cut fibre preparations, critical diffusible factors may potentially be washed out of the myoplasmic compartment, possibly precluding proper G-protein signalling. Second, GTPγS will indiscriminately activate all G-protein signalling in the cell, thus complicating interpretations at the mechanistic level. Finally, along the same line, GTPγS is expected to stimulate both Gα- and G$\beta\gamma$-signalling pathways, thus further hampering the interpretation of experimental results. Interestingly, recent data on cultured myotubes showed that direct extracellular application of the calcitonin gene-related peptide (CGRP) enhanced voltage-gated Ca^{2+} release, L-type calcium currents and charge movements (Avila *et al.* 2007). This then supports a functional role of GPCRs in regulating Ca^{2+} influx through $Ca_v1.1$ and thus potentially E–C coupling.

The aim of the present study was to specifically test the role of the G-protein $\beta\gamma$ complex in the control of Ca^{2+} homeostasis in skeletal muscle fibres from mouse. We investigated the effects of the functional G-protein $\beta_1\gamma_2$ dimer on the Ca^{2+} channel properties of the DHPR, as well as on those of the voltage-activated Ca^{2+} transients in fully differentiated adult skeletal muscle fibres. Our results suggest that the G-protein $\beta_1\gamma_2$ dimer is targeted to the T-tubule membrane system where it modulates Ca^{2+} homeostasis by inhibiting the ion channel function of the DHPR and the voltage-activated SR Ca^{2+} release process. Our findings thus provide novel evidence for an efficient G-protein-dependent regulatory mechanism of E–C coupling in adult skeletal muscle.

Methods

Ethical approval

All experiments and procedures were performed in accordance with the guidelines of the local animal ethics committee of University Lyon 1, of the French Ministry of Agriculture (87/848) and of the European Community (86/609/EEC). We have read the article by Drummond (2009) and our experiments comply with the policies and regulations of *The Journal of Physiology* and UK regulations on animal experimentation.

Plasmid cDNAs

Plamid cDNAs encoding for GFP-tagged Gβ_{1-4} and Gγ_2 were created and tagged as described by us previously (Arnot *et al.* 2000; Feng *et al.* 2001).

In vivo cDNA electroporation

Experiments were performed using 4- to 8-week-old male OF1 mice (Charles River Laboratories, L'Arbresle, France). *In vivo* cDNA electroporation was performed as previously described (Weiss *et al.* 2008). Mice were anaesthetized by I.P. injection of 10 μl g^{-1} of a mixture of 5% ketamine (Merial, Lyon, France) and 2% xylazine (Bayer, Kiel, Germany). A 50 μl aliquot of 10 μg μl^{-1} of the plasmid mix cDNAs encoding for the GFP-tagged Gβ construct (GFP-Gβ_1, GFP-Gβ_2, GFP-Gβ_3 or GFP-Gβ_4) along with the G-protein γ_2 subunit was injected within the ventral side of the posterior paws through a 29-gauge needle (Terumo, Leuven, Belgium). The paw was then placed between two flat platinum electrodes, and eight pulses of 200 V cm^{-1} amplitude of 20 ms duration were applied at 1 Hz (ECM 830 Electro Square Porator, BTX).

Isolation and preparation of FDB muscle fibres

Experiments were performed on single skeletal fibres isolated from the flexor digitorum brevis (FDB) muscles 5 days after electroporation. Procedures for enzymatic isolation of single fibres, partial insulation of the fibres with silicone grease and intracellular dye loading were as previously described (Jacquemond, 1997; Collet *et al.* 1999, 2004; Collet & Jacquemond, 2002). In brief, mice were killed by cervical dislocation after isofluorane (Sigma Aldrich, Saint Quentin Fallavier, France) inhalation, before removal of the muscles. Muscles were treated with 2 mg ml^{-1} collagenase type-1 (Sigma Aldrich) in Tyrode solution (see Solutions) for 60 min at 37°C. Single fibres were then isolated by triturating the muscles within the experimental chamber. Fibres expressing the G$\beta_x\gamma_2$ dimers were identified from the GFP fluorescence. The major part of a single fibre was then electrically insulated with silicone grease (Rhodia Siliconi Italia, Treviolo, Italy) so that whole-cell voltage-clamp could be achieved on a short portion of the fibre extremity. As previously reported, upon expression of exogenous ryanodine receptors (Legrand *et al.* 2008) one hallmark of the expression pattern of the G$\beta\gamma$ dimers was that it was not homogenous throughout the muscle fibres but most usually restricted within one given portion of the fibres, around a nucleus. Transfected fibres thus had to be handled with silicone so that the fibre region exhibiting GFP fluorescence was left out of the silicone. However, not all GFP-positive fibres were amenable to this procedure, especially when the region of expression was within the

central portion of the fibre. More importantly, in most cases the total portion of fibre left out of silicone was not 100% GFP-positive so that any effect due to the expressed G$\beta\gamma$ dimer was likely to be underestimated in the silicone-free portion of the fibre for measurements of whole-cell membrane currents and indo-1 fluorescence.

Confocal imaging

Confocal images of the GFP fluorescence and di-8-ANEPPS (10 μM, Invitrogen) labelling on freshly isolated fibres were obtained on a Zeiss LSM 5 laser scanning confocal microscope. The microscope was equipped with a $\times$63 oil immersion objective (numerical aperture 1.4). All experiments were performed at room temperature (20–22°C).

Electrophysiology

An RK-400 patch-clamp amplifier (Bio-logic, Claix, France) was used in whole-cell configuration. Command voltage pulse generation and data acquisition were done using WinWCP software (freely provided by Dr Dempster, University of Strathclyde, Glasgow, UK) driving an A/D, D/A converter (National Instruments, Austin, TX, USA). Analog compensation was systematically used to decrease the effective series resistance. Voltage-clamp was performed with a microelectrode filled with an internal-like solution (see Solutions) of 1–3 MΩ resistance. The tip of the microelectrode was inserted through the silicone within the insulated part of the fibre. Membrane depolarization were applied every 30 s from a holding command potential of -80 mV. A 30 s pulse interval allows the total recovery of DHPRs from the inactivated state (Collet *et al.* 2003).

Measurement of calcium currents

Voltage-activated Ca^{2+} currents were recorded in response to 1-s-long depolarizing steps to various potentials. The linear leak component of the current was removed by subtracting the adequately scaled value of the steady current measured during a 20 mV hyperpolarizing step applied before each test pulse. The voltage dependence of the peak Ca^{2+} current density was fitted with the following modified Boltzman equation:

$$I(V) = G_{\max}(V - V_{\text{rev}})/(1 + \exp[(V_{1/2} - V)/k]$$

with $I(V)$ being the peak current density at the command potential V, $G_{\max}$ the maximum conductance, V_{rev} the reversal potential, $V_{1/2}$ the half-activation potential and k the steepness factor. The voltage dependence of the whole-cell Ca^{2+} conductance was calculated using the following modified Boltzman equation:

$$G(V) = G_{\max}/(1 + \exp(-(V - V_{1/2})/k))$$

with $G(V)$ being the Ca^{2+} conductance at the command potential V.

Measurement of intramembrane charge movement

Charge movement currents were measured and analysed according to previously described procedures (Collet *et al.* 2003; Pouvreau & Jacquemond, 2005). In brief, adequately scaled control current records elicited by 50-ms-long hyperpolarizing pulses of 20 mV from a holding potential of -100 mV were subtracted from the current elicited by test depolarizing pulses of the same duration to levels ranging between -80 and $+20$ mV. The amount of charge moved during a test pulse was measured by integrating the 'on' portion of the corrected test current record. The calculated charge was normalized to the capacitance of the fibre. The steady-state distribution of the normalized charge was fitted with a two-state Boltzmann function: $Q(V) = Q_{\max}/\{1 + \exp[(V_{1/2} - V)/k]$, where $Q_{\max}$ corresponds to the maximal available charge, $V_{1/2}$ to the voltage of equal charge distribution and k to the steepness factor.

Ca^{2+} transients measurements using indo-1

Prior to voltage-clamp, the indo-1 dye, diluted at a concentration of 0.2 mM in an intracellular-like solution (see Solutions), was dialysed into the fibre cytoplasm through the microelectrode inserted through the silicone, within the insulated part of the fibre. In order to ease intracellular dialysis, the electrode tip was crushed within the silicon-insulated portion of the fibre by pushing it back and forth a few times towards the bottom of the chamber. Intracellular equilibration of the solution was allowed for a period of 30 min before initiating measurements. Indo-1 fluorescence was measured on an inverted Nikon Diaphot epifluorescence microscope equipped with a commercial optical system, allowing the simultaneous detection of fluorescence at 405 nm (F_{405}) and 485 nm (F_{485}) by two photomultipliers (IonOptix, Milton, MA, USA) upon 360 nm excitation. Background fluorescence at both emission wavelengths was measured next to each fibre tested and was then subtracted from all measurements.

Calibration of the indo-1 response and $[Ca^{2+}]_{\text{intra}}$ calculation

The standard ratio method was used with the parameters: $R = F_{405}/F_{485}$, with $R_{\min}$, $R_{\max}$, K_{D} and β having their usual definitions. Results were either expressed in terms of indo-1% saturation or in actual free Ca^{2+} concentration

(for details of calculation see Jacquemond, 1997; Csernoch *et al.* 1998). *In vivo* values for R_{min}, R_{max} and β were measured using procedures previously described (Collet *et al.* 1999; Collet & Jacquemond, 2002). Corresponding mean values were 0.239 ± 0.004 ($n = 9$), 1.783 ± 0.028 ($n = 9$) and 2.128 ± 0.014 ($n = 13$), respectively. No correction was made for indo-1–Ca^{2+} binding and dissociation kinetics. As a consequence, the calculated Ca^{2+} transients do not scrupulously reflect the true time course of change in free calcium. This, however, will not influence any of the conclusions from the present study (for details, see Jacquemond, 1997).

Solutions

The intracellular-like solution contained (in mM): 120 potassium glutamate, 5 Na_2-ATP, 5 Na_2-phosphocreatine, 5.5 $MgCl_2$, 5 D-glucose and 5 Hepes adjusted to pH 7.2 with KOH. The standard extracellular solution contained (in mM): 140 TEA-methanesulphonate, 2.5 $CaCl_2$, 2 $MgCl_2$, 0.002 TTX and 10 Hepes, adjusted to pH 7.2. For measurement of the slow Ca^{2+} current, the extracellular solution also contained 1 mM 4-aminopyridine and 5 $CaCl_2$, and fibres were incubated with 0.1 mM EGTA-AM for 30 min before starting the experiment. The Tyrode solution contained (in mM): 140 NaCl, 5 KCl, 2.5 $CaCl_2$, 2 $MgCl_2$ and 10 Hepes, adjusted to pH 7.2 with NaOH. For measurements of charge movement the extracellular solution contained (in mM): 140 TEA-methanesulphonate, 0.5 $CaCl_2$, 4 $MgCl_2$, 1 4-aminopyridine, 1 $CdCl_2$, 1 $CoCl_2$, 10 TEA-Hepes and 0.002 tetrodotoxin, pH 7.2. In addition, fibres were pressure-microinjected with a solution containing 50 mM EGTA diluted in the intracellular-like solution.

Statistics

Least-squares fits were performed using a Marquardt–Levenberg algorithm routine included in Microcal Origin (OriginLab, Northampton, MA, USA). Data values are presented as mean ± S.E.M. for n fibres tested, where n is specified in Results. Statistical significance was determined using Student's t test: $^{*}P < 0.05$; $^{**}P < 0.01$; $^{***}P < 0.001$; NS, statistically not different.

Results

In vivo expression of the GFP-tagged G-protein $\beta_1\gamma_2$ dimer in adult mouse skeletal muscle fibres

Under the conditions of fibre electroporation used in this study (for details see Methods), a restricted number of fibres (typically 10 to 20) were found to express the G-protein β_1–GFPγ_2 dimer out of the total population of fibres isolated from one given transfected FDB muscle. Figure 1 shows an example of the typical expression pattern of the GFP–G$\beta_1\gamma_2$ dimer observed under confocal microscopy. The GFP–G$\beta_1\gamma_2$ dimer yielded a repetitive double-row pattern perpendicular to the longitudinal axis of the fibre, consistent with the T-tubule membrane system. This was confirmed by the strong co-localization of the GFP fluorescence with the di-8-ANNEPS membrane straining (Fig. 1*C–D*). These observations indicate the proper localization of the G-protein $\beta_1\gamma_2$ dimer with regard to the excitation–contraction coupling machinery (Tanaka *et al.* 2000).

In vivo expression of the GFP-tagged G-protein $\beta_1\gamma_2$ dimer reduces L-type calcium current density

To investigate the effect of G-protein $\beta_1\gamma_2$ dimer on the ionic properties of the $Ca_v1.1$ calcium channel, L-type calcium currents were recorded in G-protein $\beta_1\gamma_2$ dimer-expressing fibres. Representative Ca^{2+} current traces recorded in response to 1 s depolarizing steps to values ranging between −50 mV and +80 mV, from a holding potential of −80 mV, are shown in Fig. 2*A* in a control fibre (left panel) and in a G$\beta_1\gamma_2$ dimer-expressing fibre (right panel). Control fibres were GFP-negative fibres issued from the same muscles. Figure 2*B* shows the mean peak Ca^{2+} current density as a function of membrane voltage for control (filled circles) and G$\beta_1\gamma_2$ dimer-expressing fibres (open circles). The L-type Ca^{2+} current density was significantly reduced in fibres expressing the G$\beta_1\gamma_2$ dimer. For instance, in response to a depolarizing pulse to +10 mV, the mean peak Ca^{2+} current density was decreased by 40% ($P = 0.0004$) in G$\beta_1\gamma_2$-expressing fibres (-5.9 ± 1.1 A/F, $n = 6$) compared to control fibres (-9.8 ± 0.4 A/F, $n = 25$). The voltage dependence of the L-type Ca^{2+} current activation was also determined in control and in G$\beta_1\gamma_2$-expressing fibres (Fig. 2*B*, inset). The mean half-activation potential remained unaltered ($P = 0.26$) in G$\beta_1\gamma_2$-expressing fibres (-2.3 ± 2.8 mV, $n = 6$) compared to control fibres (-5.0 ± 0.9 mV, $n = 25$). The mean corresponding conductance *versus* membrane potential relationships are presented in Fig. 2*C* for control fibres (filled circles) and G$\beta_1\gamma_2$-expressing fibres (open circles). The maximal conductance (Fig. 2*C*, inset) was reduced by 35% ($P = 0.001$) in G$\beta_1\gamma_2$-expressing fibres (103 ± 11 S/F, $n = 6$) as compared to control fibres (159 ± 7 S/F, $n = 25$). Electroporation itself had no effect on the L-type Ca^{2+} current density (data not shown). We also tested the capability of other G-protein β subunit isoforms to modulate L-type Ca^{2+} currents. Representative current traces from fibres expressing G$\beta_2\gamma_2$ (top panel), G$\beta_3\gamma_2$ (middle panel) and G$\beta_4\gamma_2$ (bottom panel) are shown in

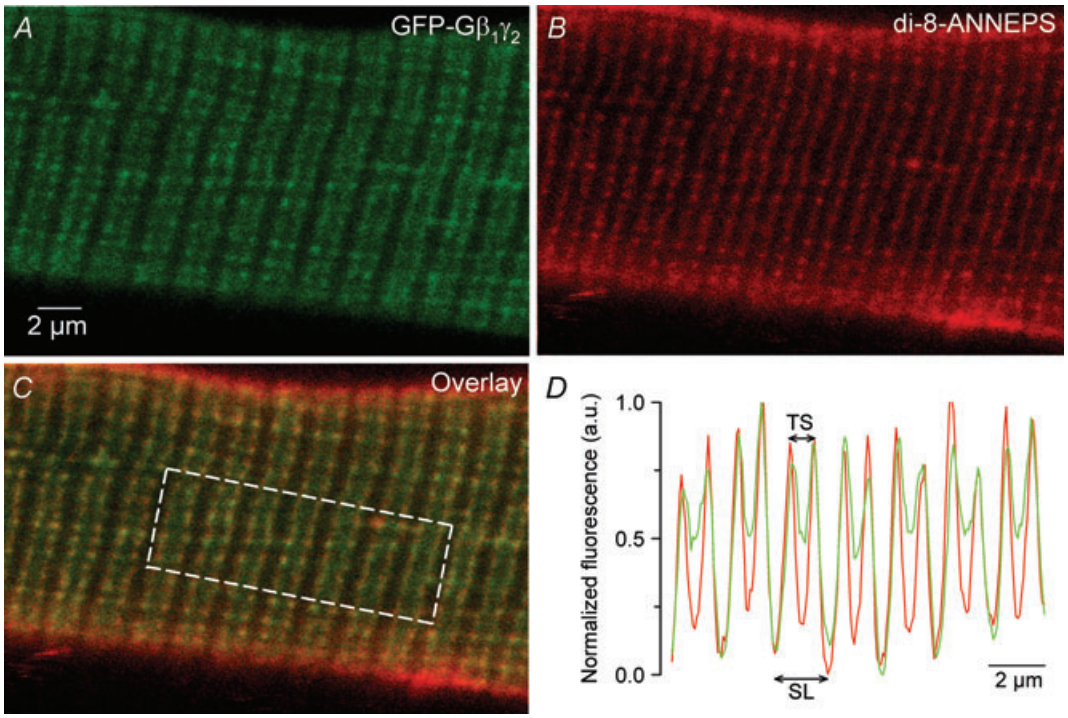

Figure 1. Expression of the GFP-tagged $G\beta_1\gamma_2$ dimer in adult muscle fibres
A, confocal images of the GFP fluorescence from a fibre freshly isolated from a muscle transfected with the cDNAs coding for the GFP–$G\beta_1$ fusion protein along with the $G\gamma_2$ subunit. *B*, di-8-ANNEPS staining. *C*, overlay of the two images. *D*, normalized mean fluorescence GFP and di-8-ANNEPS profile along the *x* axis of the box region superimposed on the image in *C*. GFP–$G\beta_1$ fusion protein yields subcellular localization consistent with the T-tubule membrane. TS, T-tubule spacing; SL, sarcomere length.

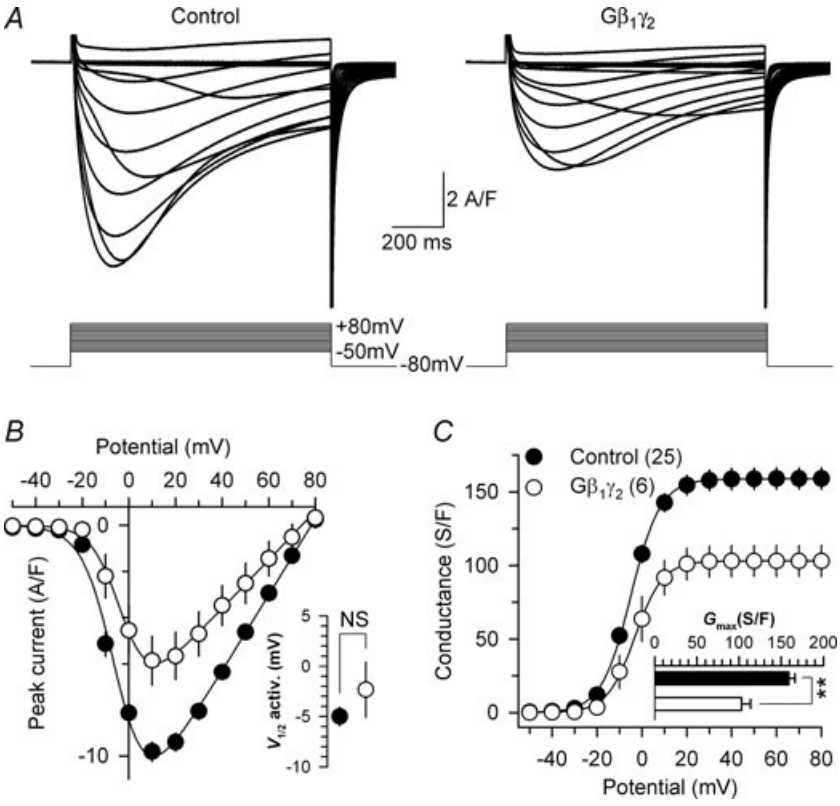

Figure 2. Expression of G-protein $\beta_1\gamma_2$ dimers reduces L-type calcium current density in skeletal muscle fibres
A, representative sets of Ca^{2+} current traces recorded from a control (left panel) and from a $G\beta_1\gamma_2$ dimer-expressing fibre (right panel) in response to 1 s depolarizing steps to values ranging between −50 mV and +80 mV from a holding potential of −80 mV. *B*, corresponding mean voltage dependence of the peak Ca^{2+} current density. Inset presents the mean half-maximal activation potential for control and $G\beta_1\gamma_2$-expressing fibres. *C*, corresponding mean values for the voltage dependence of Ca^{2+} conductance in the two populations. Inset presents the mean maximal conductance for control and $G\beta_1\gamma_2$-expressing fibres. The maximal conductance was reduced by 35% ($P = 0.001$) in the $G\beta_1\gamma_2$-expressing fibres.

Fig. 3. Corresponding mean values for peak Ca^{2+} current densities and conductances as a function of membrane potential are shown in Fig. 3*B* and *C*, respectively. No significant alteration of these parameters was observed. For instance, neither the mean half-activation potential of the L-type Ca^{2+} current, nor the maximal conductance was changed. Taken together, these data demonstrate that the L-type Ca^{2+} current is specifically altered by the G-protein $\beta_1\gamma_2$ dimer in adult skeletal muscle fibres. The possibility that absence of effect of $G\beta_2\gamma_2$, $G\beta_3\gamma_2$ and $G\beta_4\gamma_2$ would result from improper localization of the dimers in regard to the DHPR was explored by examination of the corresponding GFP fluorescence patterns under confocal microscopy. Results showed that, in contrast with the GFP-$G\beta_1\gamma_2$-expressing fibres where a double-row pattern was reproducibly observed (Fig. 1), the vast majority of fibres expressing any of the three other dimers yielded a single-row pattern clearly inconsistent with the triadic

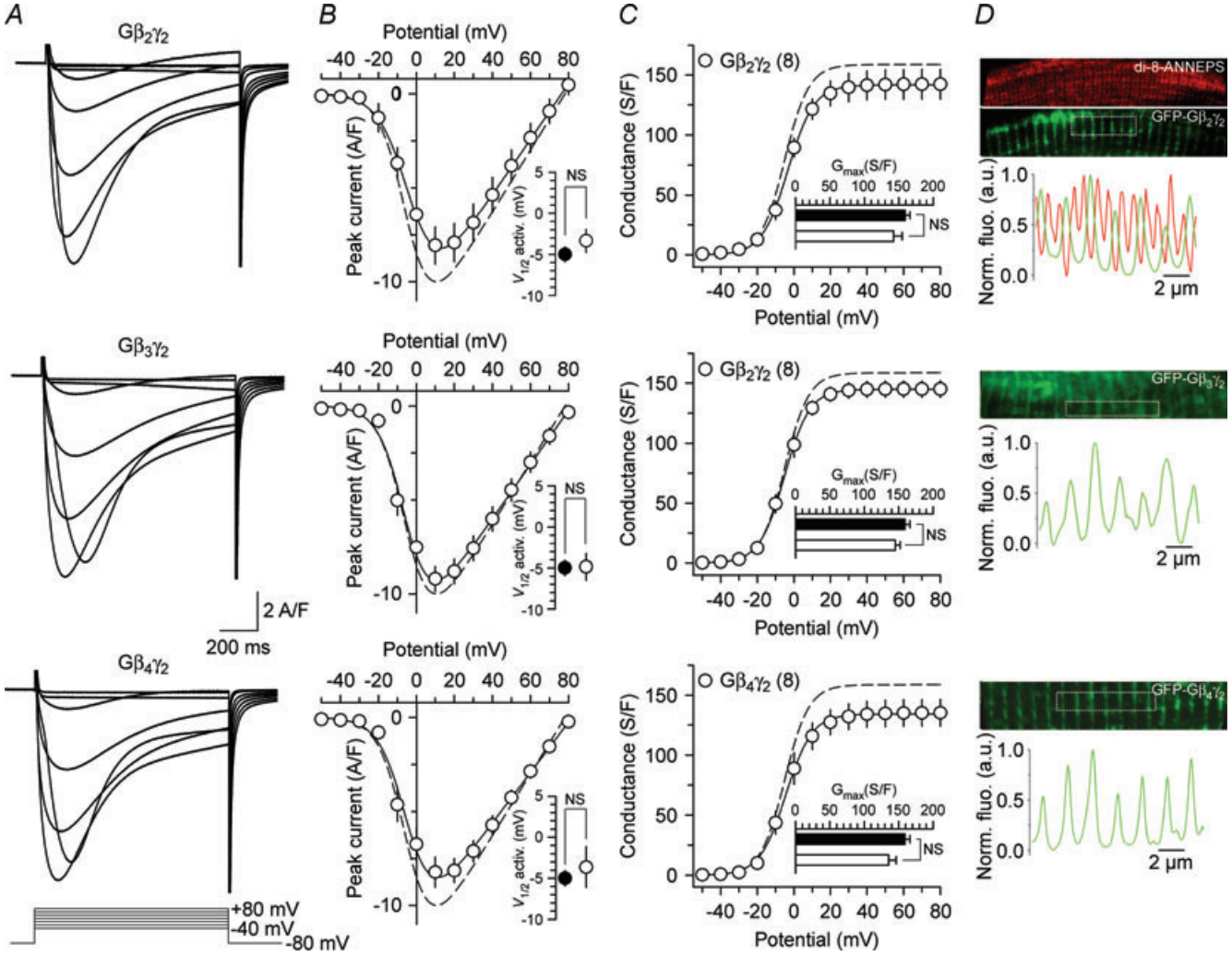

Figure 3. Expression of G-protein $\beta_2\gamma_2$, $\beta_3\gamma_2$ or $\beta_4\gamma_2$ dimers does not alter L-type calcium currents in skeletal muscle fibres

A, representative sets of Ca^{2+} current traces recorded from a $G\beta_2\gamma_2$ (top panel), $G\beta_3\gamma_2$ (middle panel) and $G\beta_4\gamma_2$ (bottom panel) -expressing fibres in response to 1 s depolarizing steps to values ranging between −40 mV and +80 mV from a holding potential of −80 mV. *B*, corresponding mean voltage dependence of the peak Ca^{2+} current density. Inset presents the mean half-maximal activation potential for $G\beta_2\gamma_2$, $G\beta_3\gamma_2$ and $G\beta_4\gamma_2$-expressing fibres. *C*, corresponding mean values for the voltage dependence of Ca^{2+} conductance in the three populations. Inset presents the mean maximal conductance for $G\beta_2\gamma_2$, $G\beta_3\gamma_2$ and $G\beta_4\gamma_2$-expressing fibres. The dashed line corresponds to the values from the control fibres. *D*, expression pattern of the GFP-tagged $G\beta_2\gamma_2$, $G\beta_3\gamma_2$ and $G\beta_4\gamma_2$ dimers in adult muscle fibres. Each panel shows a region of interest selected from a confocal image of the GFP fluorescence (green) of a fibre expressing the given $G\beta$ subunit. The fibre expressing $G\beta_2\gamma_2$ was also stained with di-8-ANNEPS and the corresponding fluorescent image is shown in red. The graph underneath each set of images shows the normalized fluorescence profile of GFP (and di-8-ANNEPS) along the *x* axis of the boxed region superimposed on each image.

region. This is illustrated in Fig. 3*D*, which shows an example of the GFP pattern (green *x, y* frame and profile) from distinct fibres expressing, from top to bottom, GFP–G$\beta_2\gamma_2$, GFP–G$\beta_3\gamma_2$ and GFP–G$\beta_4\gamma_2$, respectively. The corresponding fluorescence of di-8-ANNEPS (red *x, y* frame and profile) was also imaged in the case of the GFP–G$\beta_2\gamma_2$ example given; the GFP banded pattern was clearly out of the triadic region highlighted by di-8 ANNEPS and its frequency was half that of di-8 ANNEPS. This indicates that the proteins were retained within a different cell compartment that may be close to, or correspond to, longitudinal/endoplasmic reticulum, as was suggested for other expressed proteins in previous works (see Gensler *et al.* 2001; Volpe *et al.* 2004). We wish though to stress that this was not a completely black-and-white feature because in a restricted number of fibres expressing either GFP–G$\beta_2\gamma_2$ or GFP–G$\beta_3\gamma_2$, the GFP fluorescence was either extremely diffuse with no clear pattern or yielding a faint triadic-like double-row pattern (not illustrated). We have no interpretation for these discrepancies other than raising the possibility that parameters involved in triadic targeting of a given dimer may vary in certain fibres. Altogether we believe though that the data provide strong support for the fact that proper localization of a given G$\beta\gamma$ dimer may well be a critical condition determining its functional effect on the DHPR.

Expression of the G-protein $\beta_1\gamma_2$ dimer slows down activation and inactivation kinetics of the L-type calcium current

To further investigate the functional impact of G-protein $\beta_1\gamma_2$ expression on the $Ca_v1.1$ channel, the kinetics of L-type Ca^{2+} currents were analysed in control and G$\beta_1\gamma_2$-expressing fibres. Figure 4*A* shows normalized Ca^{2+} current traces obtained in response to 1 s depolarizing steps to +10 mV (left panel) and +30 mV (right panel) from a holding potential of −80 mV, in a control fibre and in a G$\beta_1\gamma_2$-expressing fibre. We found that the Ca^{2+} current activation was slowed in

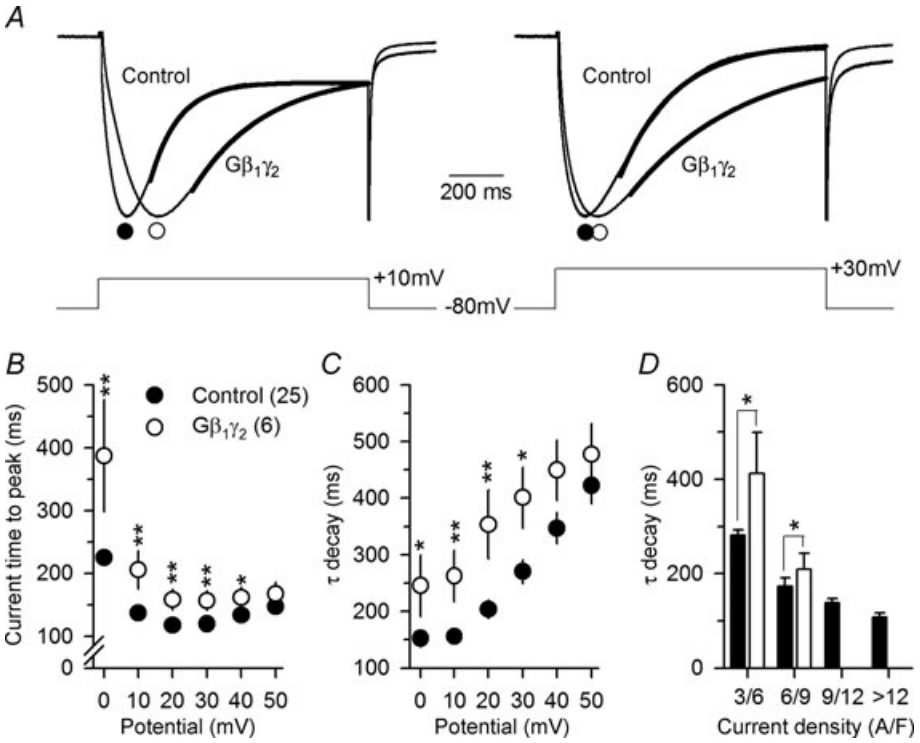

Figure 4. Expression of G-protein $\beta_1\gamma_2$ dimers slows down L-type calcium current activation and inactivation kinetics

A, normalized Ca^{2+} current traces recorded from a control and from a G$\beta_1\gamma_2$ dimer-expressing fibre in response to 1 s depolarizing steps to +10 mV (left panel) and +30 mV (right panel) from a holding potential of −80 mV. The continuous superimposed bold lines correspond to the results from fitting a single exponential function to the inactivating phase of the current. *B*, mean values for the time to peak of the Ca^{2+} current for control and G$\beta_1\gamma_2$ dimer-expressing fibres. Values were significantly increased in the G$\beta_1\gamma_2$ dimer-expressing fibres for potential values from 0 mV to +40 mV. *C*, mean values for the time constant τ of Ca^{2+} current decay. Values were significantly increased in the G$\beta_1\gamma_2$ dimer-expressing fibres at potentials ranging from 0 mV to +30 mV. *D*, dependence of the time constant of Ca^{2+} current decay at +10 mV upon the peak current density, in control and G$\beta_1\gamma_2$-expressing fibres. Values for the time constant were grouped into 4 classes of peak current density.

fibres expressing the $G\beta_1\gamma_2$ dimer as shown by larger time-to-peak values, which was particularly pronounced at the lowest voltage tested (Fig. 4*B*). For instance, in response to a depolarizing step to +10 mV, the time to peak of the Ca^{2+} current recorded from $G\beta_1\gamma_2$-expressing fibres was, on average, 1.5-fold greater than in control fibres (205 ± 30 ms, $n = 6$, *versus* 137 ± 6 ms, $n = 25$, respectively, $P = 0.001$). This slowing remained significant for depolarizing step levels up to +40 mV. The time course of Ca^{2+} current decay was determined by fitting the decay phase of the current by a single exponential function (Fig. 4*A*, bold lines). Mean corresponding values for the time constant (τ) are presented in Fig. 4*C* for control (filled circles) and $G\beta_1\gamma_2$-expressing fibres (open circles). As shown in the figure, in response to a depolarizing step to +10 mV, the time constant of Ca^{2+} current decay in $G\beta_1\gamma_2$-expressing fibres was, on average, 1.7-fold greater than in control fibres (262 ± 46 ms, $n = 6$, *versus* 156 ± 12 ms, $n = 25$, $P = 0.003$). This slowing remained significant for depolarizing step levels up to +30 mV. In adult skeletal muscle, the decay of the calcium current is believed to include a contribution from Ca^{2+} depletion from the T-tubules (see for instance Friedrich *et al.* 1999, 2001). The graph in Fig. 4*D* shows the dependence of the time constant of Ca^{2+} current decay at +10 mV upon the peak current density, for control and $G\beta_1\gamma_2$-expressing fibres. Data were grouped into four arbitrary classes of peak current density. There was a clear correlation between the time constant of current decay and the peak current density, both in control and $G\beta_1\gamma_2$-expressing fibres, consistent with the possibility that T-tubule Ca^{2+} depletion plays a role in current decay. Hence, by reducing T-tubule Ca^{2+} depletion, the decrease in Ca^{2+} conductance in $G\beta_1\gamma_2$-expressing fibres could be anticipated to contribute to the slowing of Ca^{2+} current decay. However, comparison of the mean values for the time constant of Ca^{2+} current decay between control and $G\beta_1\gamma_2$-expressing fibres within groups of fibres yielding a similar Ca^{2+} current density (3/6 and 6/9 A/F) revealed that the rate of Ca^{2+} current decay remained significantly slower in the presence of the dimer, suggesting that $G\beta_1\gamma_2$ by itself also contributes to slow down of Ca^{2+} current inactivation. The slowed decay of the Ca^{2+} current in $G\beta_1\gamma_2$-expressing fibres is thus probably the consequence of both a reduction of the Ca^{2+} conductance and an alteration of the voltage-dependent inactivation by the dimer. Since $G\beta_1\gamma_2$ slows down Ca^{2+} current inactivation, this could be thought to indirectly be the reason for the observed increased time-to-peak values of the current. However, comparison of the Ca^{2+} current time to peak between control and $G\beta_1\gamma_2$-expressing fibres for similar values of Ca^{2+} decay time constant showed that Ca^{2+} current activation remained significantly slowed in the presence of the dimer (not shown), suggesting that $G\beta_1\gamma_2$ by itself slows down Ca^{2+} current activation independently from any apparent effect due to change in the inactivation rate.

Effect of a strong depolarizing pre-pulse on the regulation of the L-type calcium current by G-protein $\beta_1\gamma_2$ dimer

It is well known that application of strong depolarizing pre-pulses on voltage-gated Ca^{2+} channels under direct G-protein regulation produces either a current facilitation, and/or a change in kinetics of the Ca^{2+} current (Scott & Dolphin, 1990; Ikeda, 1991). Representative Ca^{2+} current traces in response to a 1 s depolarizing step to +20 mV from a holding potential of −80 mV, before (P1) and after (P2) a strong 180 ms depolarizing pre-pulse to +100 mV are shown in Fig. 5*A* in a control fibre (left panel) and in a $G\beta_1\gamma_2$-expressing fibre (right panel). Figure 5*B* shows an enlarged view of the same traces after normalization to the same peak amplitude. In Fig. 5*C* the normalized peak Ca^{2+} current amplitude recorded before and after the depolarizing pre-pulse (P2/P1) was plotted as a function of the duration of the pre-pulse in control (filled circles, $n = 13$) and $G\beta_1\gamma_2$-expressing fibres (open circles, $n = 6$). Results show that there was either no pre-pulse-induced current recovery from G-protein inhibition or that the effect was sufficiently small to be masked by the inactivation of the Ca^{2+} current induced by the depolarizing pre-pulse. The time to peak of the current plotted as a function of the duration of the depolarizing pre-pulse is shown in Fig. 5*D*. Although not spectacular, there was a clear tendency for the values recorded in $G\beta_1\gamma_2$-expressing fibres to get closer to the ones recorded in control fibres as the pre-pulse duration was increased, indicative of some recovery from the process of $G\beta_1\gamma_2$-induced slowing of Ca^{2+} current activation. Figure 5*E* shows the mean values for the time constant of Ca^{2+} current decay in control fibres and in $G\beta_1\gamma_2$-expressing fibres as a function of the depolarizing pre-pulse duration. In control cells, there was a slowing of Ca^{2+} current decay upon increasing the pre-pulse duration. This slowing could be related to the reduction of the current amplitude (caused by the pre-pulse-induced current inactivation) which indirectly slows down the Ca^{2+} decay kinetics by reducing T-tubule Ca^{2+} depletion, as stated above. By contrast, in $G\beta_1\gamma_2$-expressing fibres, there was a reduction of the Ca^{2+} current decay time constant, the value of which clearly converged towards control values for the longest pre-pulse durations. The inset in Fig. 5*E* shows the same data, but values for the time constant of Ca^{2+} decay in each fibre were normalized to the value measured in the absence of pre-pulse. Effect of the pre-pulse was clearly opposite in the control fibres and in the $G\beta_1\gamma_2$-expressing ones; thus, the extent of reversion of $G\beta_1\gamma_2$-induced slowing of Ca^{2+} decay by

the pre-pulse is likely to be under-estimated because the effect observed in control fibres should also be present in the G$\beta_1\gamma_2$-expressing ones. Data thus clearly support the capability of a depolarizing pre-pulse to reverse the slowing of Ca^{2+} current inactivation induced by G$\beta_1\gamma_2$ and thus the likelihood of a direct G-protein regulation of the DHPR Ca^{2+} channel activity. Also important is the fact that depolarizing pre-pulses did not speed up Ca^{2+} current inactivation in control conditions, which suggests that DHPR channels are not under an endogenous tonic G$\beta\gamma$ regulation in control fibres. Overall, although no effect of the pre-pulses was detected on the peak current amplitude, the partial recovery from the slowing of current kinetics is consistent with the effect of the G-protein $\beta_1\gamma_2$ dimer on the L-type Ca^{2+} current to occur, at least partially, via the binding of the G$\beta_1\gamma_2$ dimer to the $Ca_v1.1$ subunit.

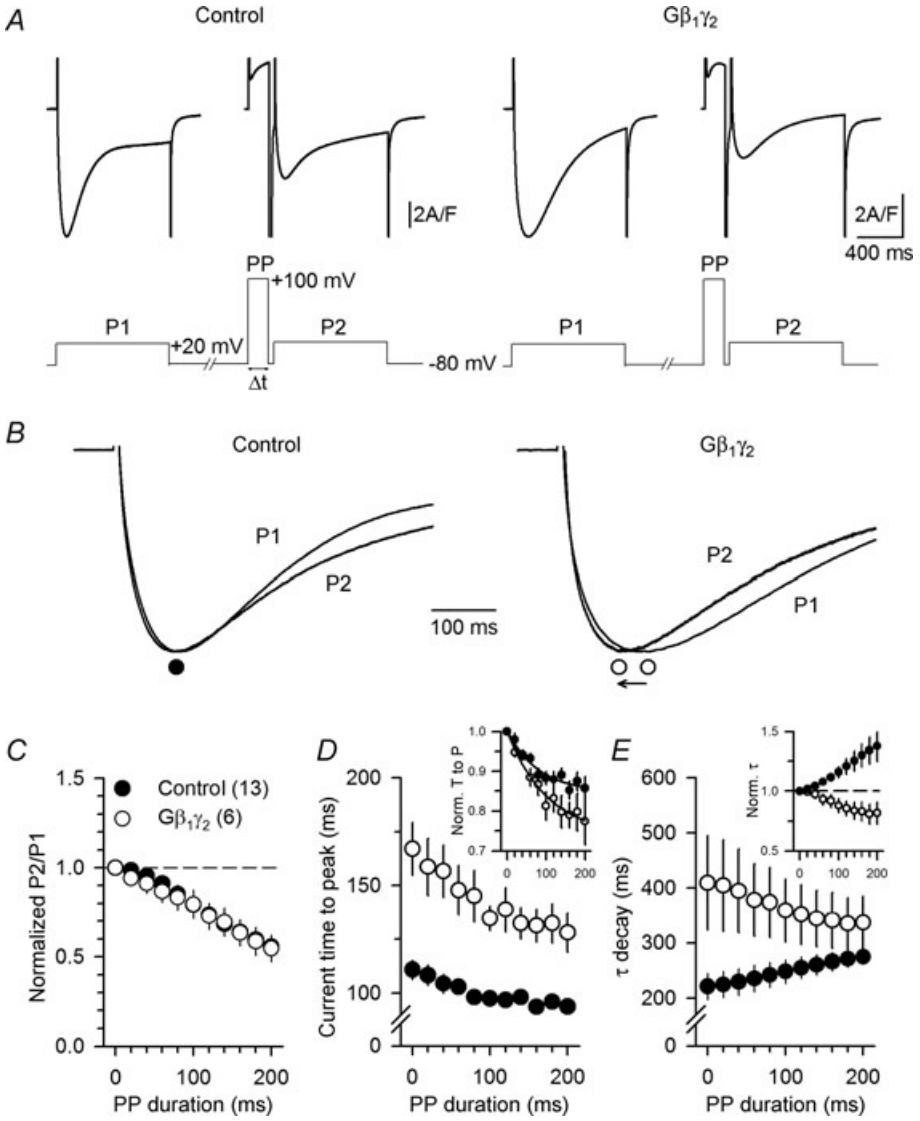

Figure 5. A strong depolarizing pre-pulse allows partial recovery from the slowing of L-type calcium current kinetics induced by G$\beta_1\gamma_2$

A, representative Ca^{2+} current traces recorded from a control (left panel) and from a G$\beta_1\gamma_2$ dimer-expressing fibre (right panel) in response to a 1 s depolarizing step to +20 mV from a holding potential of −80 mV, before (P1) and after (P2) a strong depolarizing pre-pulse (PP) to +100 mV. *B*, enlarged view of the Ca^{2+} current traces shown in *A* after normalization to the same peak amplitude, with (P2) and without (P1) pre-pulse. *C*, mean normalized values of P2/P1 peak Ca^{2+} current amplitude as a function of the pre-pulse (PP) duration. *D*, mean values for the time to peak of the Ca^{2+} current recorded in P2 as a function of the pre-pulse duration. The inset shows the corresponding mean values after normalization to the time to peak of the current measured in absence of pre-pulse. *E*, mean values for the time constant of decay of the Ca^{2+} current recorded in P2 as a function of the pre-pulse duration. The inset shows the corresponding mean values after normalization to the time constant measured in absence of pre-pulse.

G-protein $\beta_1\gamma_2$ dimer expression alters voltage-activated calcium transients

In order to further investigate the possible functional role of G-proteins in the control of excitation–contraction coupling and, from a more general point of view, in the control of intracellular Ca^{2+} homeostasis, Ca^{2+} transients were recorded in control and G$\beta_1\gamma_2$-expressing fibres under voltage-clamp conditions. Representative $[Ca^{2+}]$ traces from a control (left panel) and from a G$\beta_1\gamma_2$-expressing fibre (left panel), in response to successive depolarizing pulses of 5, 10, 20, 50 and 100 ms duration to +10 mV from a holding potential of −80 mV are shown in Fig. 6*A*. Obviously, the amplitude of the Ca^{2+} transients was dramatically diminished in the G$\beta_1\gamma_2$-expressing fibre. Figure 6*B–D* show mean values from that series of measurements for peak $\Delta[Ca^{2+}]$, time constant (τ) of $[Ca^{2+}]$ decay and final $\Delta[Ca^{2+}]$ in control (filled circle, $n = 10$) and G$\beta_1\gamma_2$-expressing fibres (open circle, $n = 6$). Measurements were performed on individual $[Ca^{2+}]$ traces calculated from each fibre. The time constant of decay was obtained by fitting a single exponential plus constant function to the $[Ca^{2+}]$ decline; the value for the constant from the fit was used to calculate the final $\Delta[Ca^{2+}]$ (Fig. 6*D*). In response to a depolarizing step of 20 ms duration, the mean peak $\Delta[Ca^{2+}]$ was 43% less ($P = 0.0003$) in G$\beta_1\gamma_2$-expressing fibres ($0.63 \pm 0.10\ \mu$M, $n = 6$) than in control ones ($1.11 \pm 0.05\ \mu$M, $n = 10$). There was no significant difference in the values for the time constant of $[Ca^{2+}]$ decay and final $\Delta[Ca^{2+}]$ level between control and G$\beta_1\gamma_2$-expressing fibres. Mean values for resting $[Ca^{2+}]$ also did not statistically differ between the two groups; for instance, the mean baseline level of $[Ca^{2+}]$ measured before the first depolarizing pulse was applied was 14.4 ± 1.3 nM and 10.9 ± 2.2 nM, in control and G$\beta_1\gamma_2$-expressing fibres, respectively. Taken together, these results indicate that expression of the G-protein $\beta_1\gamma_2$ dimer dramatically alters voltage-induced Ca^{2+} release

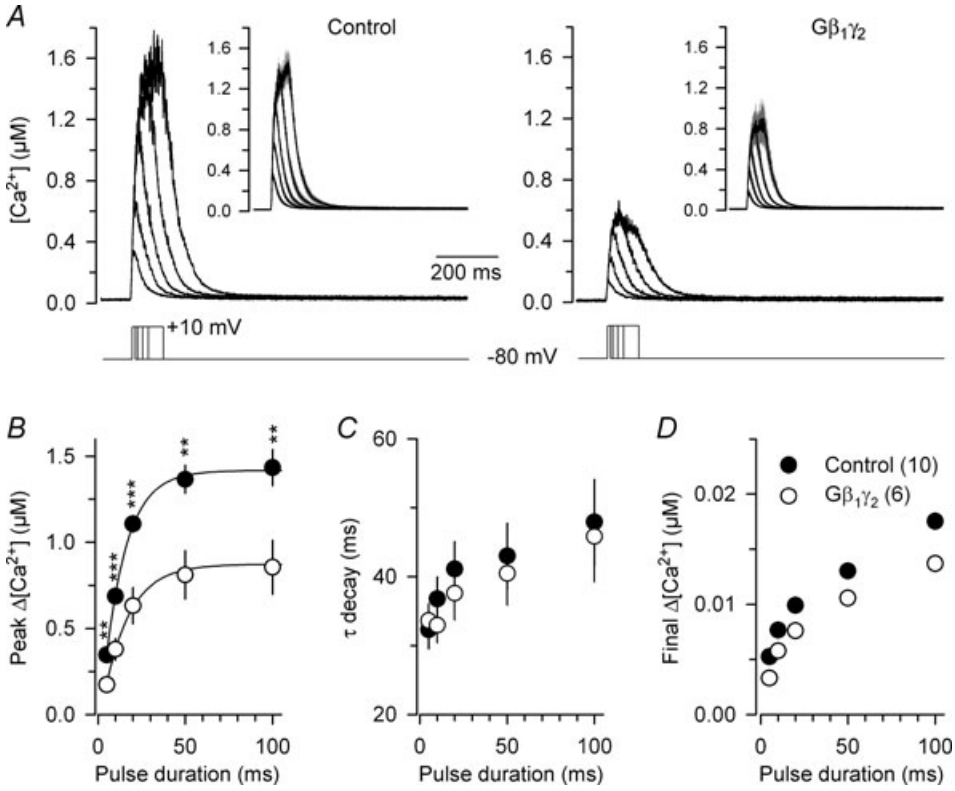

Figure 6. Expression of G-protein $\beta_1\gamma_2$ dimers strongly alters the voltage-activated Ca^{2+} transient in skeletal muscle fibres
A, representative indo-1 $[Ca^{2+}]$ traces from a control (left panel) and from a G$\beta_1\gamma_2$ dimer-expressing fibre (right panel) in response to depolarizing steps of increasing duration to +10 mV from a holding potential of −80 mV. The inset in each panel shows the corresponding mean (continuous traces) ± S.E.M. (grey shading) $[Ca^{2+}]$ traces. *B–D*, corresponding mean ± S.E.M. values of peak change in $[Ca^{2+}]$, time constant (τ) of $[Ca^{2+}]$ decay after the end of the pulse and final change in $[Ca^{2+}]$ level, respectively, measured from 10 control fibres and 6 G$\beta_1\gamma_2$ dimer-expressing fibres. The peak change in $[Ca^{2+}]$ was reduced by 43% ($P = 0.0003$) (20 ms depolarizing step) in the G$\beta_1\gamma_2$-expressing fibres. Values for the final change in $[Ca^{2+}]$ level were from the exponential fits. When not visible, errors bars are smaller than the mean dot.

without affecting the ability of the cells to regulate the Ca^{2+} concentration at rest.

Voltage sensing function of the DHPR is unaffected by the G-protein $\beta_1\gamma_2$ dimer

The question of whether the observed effects of the $\beta_1\gamma_2$ dimer on the Ca^{2+} current and on the Ca^{2+} transient were associated with a reduction of the amount of DHPR in the membrane was of most immediate interest. In order to address it, we measured intramembrane charge movement in control and G$\beta_1\gamma_2$-expressing fibres. Figure 7*A* shows illustrative traces of charge movement currents from a control fibre and from a G$\beta_1\gamma_2$-positive fibre in response to 50 ms depolarizing pulses from −100 mV to the indicated values. Altogether we found no qualitative difference between the records obtained in the two sets of fibres. Figure 7*B* shows the voltage dependence of the corresponding mean values for the 'on' charge. There was obviously no reduction of the amount of charge in the G$\beta_1\gamma_2$-expressing fibres. Fitting a two-state Boltzmann distribution to the data obtained in each fibre gave mean values for Q_{max}, $V_{1/2}$ and k of 18.4 ± 2.8 nC μF^{-1}, -29.1 ± 4.1 mV and 12.9 ± 1.8 mV in control fibres ($n = 8$), and 19.9 ± 3.7 nC μF^{-1}, -25.3 ± 3.9 mV and 15.6 ± 1.6 mV in G$\beta_1\gamma_2$-expressing fibres ($n = 5$), respectively. None of the parameters significantly differed between the two sets of fibres. Thus, despite the effect of G$\beta_1\gamma_2$ expression on the L-type Ca^{2+} current density and on the peak Ca^{2+} transient, there was no associated reduction of intramembrane

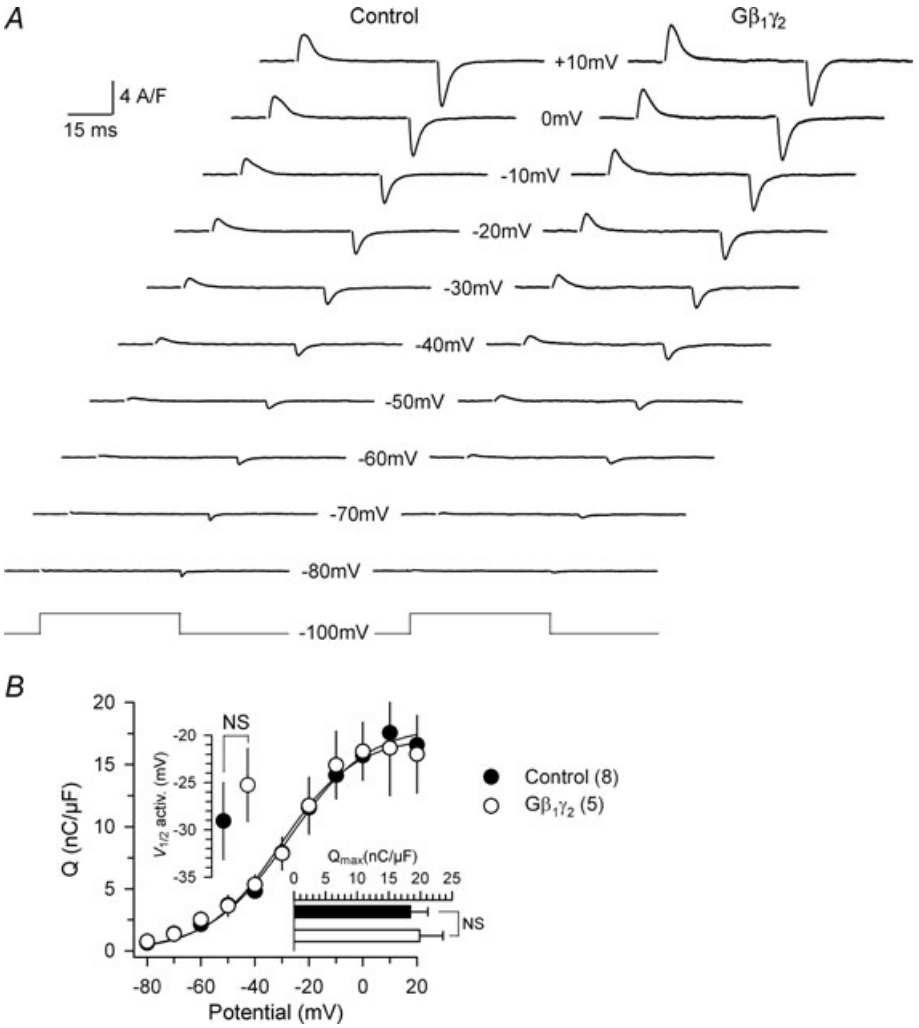

Figure 7. Intramembrane charge movement in G$\beta_1\gamma_2$-expressing fibres
A, representative charge movement records from a control fibre and from a GFP-G$\beta_1\gamma_2$-positive fibre, measured in response to 50 ms depolarizing steps to the indicated values of membrane potential. *B*, mean voltage distribution of the 'on' charge in control fibres ($n = 8$) and in GFP-G$\beta_1\gamma_2$-positive fibre ($n = 5$). Superimposed continuous lines correspond to a two-state Boltzmann distribution calculated using the mean parameters obtained from fits to the individual sets of data in the two groups of fibres (see text for details).

charge movement. The molecular mechanism(s) targeted by G$\beta_1\gamma_2$ thus has to lie beyond the voltage-sensing steps of the DHPR.

Discussion

We demonstrate that expression of the G-protein $\beta_1\gamma_2$ dimer in intact adult mammalian skeletal muscle fibres alters both the Ca^{2+} channel function of the DHPR and the process of voltage-activated Ca^{2+} release from the SR. These results provide strong support for the ability of $Ca_v1.1$ proteins to undergo G-protein inhibition. *In vivo* expression of the G-protein $\beta_1\gamma_2$ dimer in adult mouse muscle was successful and yielded a very distinct subcellular pattern consistent with a specific localization of the dimer in the T-tubule membrane system. This is in accordance with previous biochemical studies showing the presence of the G-protein β subunits in T-tubule membrane preparations purified from rabbit skeletal muscle (Toutant *et al.* 1988), as well as with immunostaining of endogenous G-protein β subunits, also in rabbit skeletal muscle (Toutant *et al.* 1990). A clear T-tubule consistent pattern could, however, not be reproducibly observed upon expression of either the $\beta_2\gamma_2$, the $\beta_3\gamma_2$ or the $\beta_4\gamma_2$ dimers, which were all found to also have no effect on the DHPR Ca^{2+} channel function. Although we cannot completely exclude that functional properties specific to the Gβ_1 subtype play a role in the observed regulation of the DHPR, proper targeting in the T-tubule membrane may well be a critical parameter determining the efficiency of Gβ_1. One could then also speculate that the $\beta_1\gamma_2$ dimer acts through a disruptive non-specific effect only related to its over-expression in that particular restricted area of the muscle fibres. However, we previously showed that over-expression of wild-type caveolin-3 (Couchoux *et al.* 2007) or of the C71W mutant form of caveolin-3 (Weiss *et al.* 2008), which both localize in the T-tubule membrane, have no effect on the DHPR Ca^{2+} current. We thus believe that the possibility of a non-specific effect is quite unlikely.

Possible mechanism of G-protein $\beta_1\gamma_2$ modulation of the L-type Ca^{2+} current

Previous studies aiming at exploring the role of G-proteins on E–C coupling in adult muscle used GTPγS on either skinned skeletal muscle fibre preparations (Di Virgilio *et al.* 1986; Lamb & Stephenson, 1991; Somasundaram *et al.* 1991) or vaseline-gap voltage-clamped cut fibres (Garcia *et al.* 1990), which provided controversial results. As detailed earlier, the use of GTPγS under such conditions is a somewhat limiting strategy. In this context, the *in vivo* expression of exogenous functional G-protein $\beta_1\gamma_2$ dimer in intact fully differentiated muscle fibres provides a more defined and specific approach. In particular, it should bypass the possible consequences of activation of multiple endogenous G-protein signalling pathways.

On average, G$\beta_1\gamma_2$ positive fibres yielded a decrease in Ca^{2+} current amplitude corresponding to a 35% drop in peak conductance. This is a very substantial alteration, especially considering that it is likely to be heavily underestimated because of the local expression of the G$\beta_1\gamma_2$ dimer within the whole-cell voltage-clamped portion of fibre (see Methods). Of importance, we found no alteration of intramembrane charge movement in the G$\beta_1\gamma_2$-expressing fibres, demonstrating that the reduction of Ca^{2+} current density was not due to a loss of DHPR in the T-tubule membrane and that the overall effects of G$\beta_1\gamma_2$ did not involve an alteration of the voltage-sensing steps of the DHPR function. This also excludes the possibility that inhibition in DHPR current would have resulted from G$\beta_1\gamma_2$ increasing expression of Rem/Gem-related proteins, previously shown to inhibit DHPR channel and voltage-sensing function by reducing DHPR expression (Bannister *et al.* 2008). Conversely, we cannot totally exclude that over-expression of G$\beta_1\gamma_2$ could sequestrate a tonic stimulatory effect of Gα subunit since it was demonstrated that $Ca_v1.1$ channel in cultured muscle cells is modulated by the cAMP-dependent protein kinase (Johnson *et al.* 1997). Still, there is to our knowledge very limited, if any, indication that this is also true in adult muscle fibres. Furthermore, if such a mechanism took place, we could well expect observing the same phenomenon in G$\beta_2\gamma_2$-, G$\beta_3\gamma_2$- and G$\beta_4\gamma_2$-expressing fibres, which clearly was not the case.

The G-protein $\beta\gamma$ dimer is known to directly regulate neuronal voltage-gated Ca^{2+} channels ($Ca_v2.1$, $Ca_v2.2$ and $Ca_v2.3$) (for review, see De Waard *et al.* 2005; Tedford & Zamponi, 2006) through direct binding of the G$\beta\gamma$ dimer onto various structural elements of the $Ca_v2.x$ subunit. Those include the loop linking transmembrane domains I and II (De Waard *et al.* 1997; Zamponi *et al.* 1997), the amino-terminal (Agler *et al.* 2005) and possibly the carboxy-terminal domain (Qin *et al.* 1997). Our results showing a pre-pulse-dependent reversal of some of the kinetic effects suggest that $Ca_v1.1$ L-type channels can also be directly regulated by G-proteins, although we do not presently have biochemical evidence to demonstrate a protein–protein interaction. It should be remembered that complete absence of effects of pre-pulses would, though, not have been sufficient to exclude a direct regulation, as for instance $Ca_v3.2$ channels were shown to be specifically regulated by the G$\beta_2\gamma_2$ dimer through direct binding onto the intracellular loop linking domains II and III of the channel, the regulation being though totally insensitive to a strong depolarizing pre-pulse (Wolfe *et al.* 2003). Also worth mentioning is the fact that $Ca_v1.x$ channels were initially thought not to be regulated by direct G-protein interaction because they lack the G$\beta\gamma$

binding QXXER motif present in the I–II loop of $Ca_v2.x$ channels. However, more recently, it was demonstrated that the $Ca_v1.2$ channel is sensitive to G-protein inhibition through a direct binding of the $G\beta\gamma$ dimer onto the amino- and carboxy-terminal domains of the channel (Ivanina *et al.* 2000).

The so far limited amount of evidence concerning G-protein regulation of $Ca_v1.1$ L-type channels is probably related to difficulty in heterologous expression of $Ca_v1.1$ channels. Here, the fully differentiated skeletal muscle fibre preparation allowed detailed investigation of the role of the G-protein $\beta\gamma$ dimer on the $Ca_v1.1$ channel activity. Although we cannot totally exclude that over-expression of $G\beta_1\gamma_2$ may have activated another signal transduction pathway to modulate $Ca_v1.1$ activity, several considerations argue against such a mechanism. First, the effect is specific as only the G-protein β_1 subunit modulated channel activity. This is reminiscent of data obtained with the $Ca_v3.2$ T-type channel that was shown to be solely mediated by the G-protein β_2 subunit, with other $G\beta$ subunits being ineffective (Wolfe *et al.* 2003; DePuy *et al.* 2006). Second, the slowing of activation and inactivation kinetics of L-type Ca^{2+} currents in $G\beta_1\gamma_2$-expressing fibres, and its reversal by a depolarizing pre-pulse, fits with the idea of direct G-protein regulation (Marchetti *et al.* 1986; Scott & Dolphin, 1990; Ikeda, 1991; Zamponi, 2001). Finally, previous biochemical studies suggested that the G-protein β subunit associates with the DHPR, although the molecular determinants involved in this interaction remained unidentified (Hamilton *et al.* 1991). Altogether, we favour the idea of a direct G-protein regulation of the DHPR Ca^{2+} channel activity.

Possible mechanism of G-protein $\beta_1\gamma_2$ modulation of the excitation–contraction coupling

Functional coupling between the DHPR and RyR1 occurs through direct or indirect interactions of possibly several cytosolic determinants of $Ca_v1.1$ with RyR1 (for recent review see Bannister, 2007). Among them the II–III loop is established to play a key role in E–C coupling (Tanabe *et al.* 1990; Lu *et al.* 1994) and alteration of the corresponding interaction alters both the L-type Ca^{2+} current density and the amplitude of the voltage-activated Ca^{2+} transient (Bannister *et al.* 2009). Other structural determinants of the $Ca_v1.1$ subunit postulated to be involved in the regulation of E–C coupling include the I–II loop (via the voltage-gated Ca^{2+} channel β_{1a} subunit (Gregg *et al.* 1996; Strube *et al.* 1996), the carboxy-terminal domain (Slavik *et al.* 1997; Sencer *et al.* 2001) and, although probably less critical, the III–IV loop (Leong & MacLennan, 1998; Weiss *et al.* 2004). As there is no evidence of G-protein $\beta\gamma$ dimer interaction with RyR1, the inhibition of voltage-activated Ca^{2+} release observed in the $G\beta_1\gamma_2$-expressing fibres is probably not the consequence of a direct regulation of RyR1, but may instead be mediated by the binding of the dimer to the $Ca_v1.1$ subunit. Moreover, our observation that the expression of G-protein $\beta_1\gamma_2$ dimer alters both the L-type Ca^{2+} current and the voltage-activated Ca^{2+} release is suggestive of a common regulation mechanism. It is well known that the interaction of the II–III loop of the $Ca_v1.1$ subunit with RyR1 is responsible for a bidirectional coupling: (i) an orthograde coupling characterized by a voltage-induced Ca^{2+} release via RyR1, and (ii) a retrograde coupling manifested by an increase of the L-type Ca^{2+} current via the DHPR (Grabner *et al.* 1999). Hence, it is tempting to propose that the G-protein $\beta_1\gamma_2$ dimer may control simultaneously the L-type Ca^{2+} current and the voltage-activated Ca^{2+} release by modulating the bidirectional coupling between the DHPR and RyR1.

Potential physiological consequences of $G\beta_1\gamma_2$ modulation of $Ca_v1.1$

Our data raise the intriguing possibility that the $G\beta_1\gamma_2$-mediated inhibition of E–C coupling revealed here could be triggered by the activation of specific GPCRs that are coupled selectively to $G\beta_1\gamma_2$. This could obviously be of very strong relevance for the regulation of muscle function. Many GPCRs are expressed or presumably expressed in skeletal muscle, some of them being devoid of known agonists (Jean-Baptiste *et al.* 2005). So far only the calcitonin gene-related peptide (CGRP) was shown to be effective in the muscle E–C coupling context, stimulating both DHPR Ca^{2+} current and Ca^{2+} release (Avila *et al.* 2007). However, results were obtained on cultured myotubes, i.e immature cells in the process of maturation and differentiation. Under these conditions, it is difficult to assess whether CGRP accelerates the process of maturation/differentiation or if it acutely regulates the E–C coupling process. The time course of the reported CGRP action (several hours), and the fact that effects were attenuated at later time during myotube differentiation actually favoured a maturation effect.

Identification of GPCRs involved in G-protein-mediated inhibition of E–C coupling, and of their respective extracellular agonists thus still represents a challenging task. Finally, a functional association of G-protein $\beta\gamma$ dimer with the dystrophin glycoprotein complex (DGC) was shown to be present in skeletal muscle (Xiong *et al.* 2009). One then could raise the possibility that disruption of the DGC in muscular dystrophies (for review see Durbeej & Campbell, 2002) may release free $G\beta\gamma$ dimer, which in turn could alter Ca^{2+} homeostasis and excitation–contraction coupling and contribute to muscle diseases.

Overall, our data constitute the first description of $Ca_v1.1$ modulation by G-protein $\beta\gamma$ subunits. While

further work will be required to ascertain its consequences for E–C coupling, the direct modulation of $Ca_v1.1$ by this pathway may provide a previously unrecognized means of regulating muscle physiology.

References

Agler HL, Evans J, Tay LH, Anderson MJ, Colecraft HM & Yue DT (2005). G protein-gated inhibitory module of N-type $Ca_v2.2$ Ca^{2+} channels. *Neuron* **46**, 891–904.

Arnot MI, Stotz SC, Jarvis SE & Zamponi GW (2000). Differential modulation of N-type 1B and P/Q-type 1A calcium channels by different G protein subunit isoforms. *J Physiol* **527**, 203–212.

Avila G, Aguilar CI & Ramos-Mondragon R (2007). Sustained CGRP1 receptor stimulation modulates development of EC coupling by cAMP/PKA signalling pathway in mouse skeletal myotubes. *J Physiol* **584**, 47–57.

Bannister RA (2007). Bridging the myoplasmic gap: recent developments in skeletal muscle excitation-contraction coupling. *J Muscle Res Cell Motil* **28**, 275–283.

Bannister RA, Colecraft HM & Beam KG (2008). Rem inhibits skeletal muscle EC coupling by reducing the number of functional L-type Ca^{2+} channels. *Biophys J* **94**, 2631–2638.

Bannister RA, Papadopoulos S, Haarmann CS & Beam KG (2009). Effects of inserting fluorescent proteins into the α1S II-III loop: insights into excitation-contraction coupling. *J Gen Physiol* **134**, 35–51.

Collet C, Allard B, Tourneur Y & Jacquemond V (1999). Intracellular calcium signals measured with indo-1 in isolated skeletal muscle fibres from control and mdx mice. *J Physiol* **520**, 417–429.

Collet C, Csernoch L & Jacquemond V (2003). Intramembrane charge movement and L-type calcium current in skeletal muscle fibers isolated from control and mdx mice. *Biophys J* **84**, 251–265.

Collet C & Jacquemond V (2002). Sustained release of calcium elicited by membrane depolarization in ryanodine-injected mouse skeletal muscle fibers. *Biophys J* **82**, 1509–1523.

Collet C, Pouvreau S, Csernoch L, Allard B & Jacquemond V (2004). Calcium signaling in isolated skeletal muscle fibers investigated under "silicone voltage-clamp" conditions. *Cell Biochem Biophys* **40**, 225–236.

Couchoux H, Allard B, Legrand C, Jacquemond V & Berthier C (2007). Loss of caveolin-3 induced by the dystrophy-associated P104L mutation impairs L-type calcium channel function in mouse skeletal muscle cells. *J Physiol* **580**, 745–754.

Csernoch L, Bernengo JC, Szentesi P & Jacquemond V (1998). Measurements of intracellular Mg^{2+} concentration in mouse skeletal muscle fibers with the fluorescent indicator mag-indo-1. *Biophys J* **75**, 957–967.

De Waard M, Hering J, Weiss N & Feltz A (2005). How do G proteins directly control neuronal Ca^{2+} channel function? *Trends Pharmacol Sci* **26**, 427–436.

De Waard M, Liu H, Walker D, Scott VE, Gurnett CA & Campbell KP (1997). Direct binding of G-protein $\beta\gamma$ complex to voltage-dependent calcium channels. *Nature* **385**, 446–450.

DePuy SD, Yao J, Hu C, McIntire W, Bidaud I, Lory P, Rastinejad F, Gonzalez C, Garrison JC & Barrett PQ (2006). The molecular basis for T-type Ca^{2+} channel inhibition by G protein $\beta2\gamma2$ subunits. *Proc Natl Acad Sci U S A* 103, 14590–14595.

Di Virgilio F, Salviati G, Pozzan T & Volpe P (1986). Is a guanine nucleotide-binding protein involved in excitation-contraction coupling in skeletal muscle? *EMBO J* **5**, 259–262.

Drummond GB (2009). Reporting ethical matters in *The Journal of Physiology*: standards and advice. *J Physiol* **587**, 713–719.

Dulhunty AF (2006). Excitation-contraction coupling from the 1950s into the new millennium. *Clin Exp Pharmacol Physiol* **33**, 763–772.

Durbeej M & Campbell KP (2002). Muscular dystrophies involving the dystrophin-glycoprotein complex: an overview of current mouse models. *Curr Opin Genet Dev* **12**, 349–361.

Feng ZP, Arnot MI, Doering CJ & Zamponi GW (2001). Calcium channel b subunits differentially regulate the inhibition of N-type channels by individual Gb isoforms. *J Biol Chem* **276**, 45051–45058.

Friedrich O, Ehmer T & Fink RH (1999). Calcium currents during contraction and shortening in enzymatically isolated murine skeletal muscle fibres. *J Physiol* **517**, 757–770.

Friedrich O, Ehmer T, Uttenweiler D, Vogel M, Barry PH & Fink RH (2001). Numerical analysis of Ca^{2+} depletion in the transverse tubular system of mammalian muscle. *Biophys J* **80**, 2046–2055.

Garcia J, Gamboa-Aldeco R & Stefani E (1990). Charge movement and calcium currents in skeletal muscle fibers are enhanced by GTPγS. *Pflugers Arch* **417**, 114–116.

Gensler S, Sander A, Korngreen A, Traina G, Giese G & Witzemann V (2001). Assembly and clustering of acetylcholine receptors containing GFP-tagged ε or γ subunits: selective targeting to the neuromuscular junction *in vivo*. *Eur J Biochem* **268**, 2209–2217.

Grabner M, Dirksen RT, Suda N & Beam KG (1999). The II-III loop of the skeletal muscle dihydropyridine receptor is responsible for the bi-directional coupling with the ryanodine receptor. *J Biol Chem* **274**, 21913–21919.

Gregg RG, Messing A, Strube C, Beurg M, Moss R, Behan M *et al.* (1996). Absence of the β subunit (cchb1) of the skeletal muscle dihydropyridine receptor alters expression of the α1 subunit and eliminates excitation-contraction coupling. *Proc Natl Acad Sci USA* **93**, 13961–13966.

Hamilton SL, Codina J, Hawkes MJ, Yatani A, Sawada T, Strickland FM *et al.* (1991). Evidence for direct interaction of Gs α with the Ca^{2+} channel of skeletal muscle. *J Biol Chem* **266**, 19528–19535.

Ikeda SR (1991). Double-pulse calcium channel current facilitation in adult rat sympathetic neurones. *J Physiol* **439**, 181–214.

Ivanina T, Blumenstein Y, Shistik E, Barzilai R & Dascal N (2000). Modulation of L-type Ca^{2+} channels by gβ γ and calmodulin via interactions with N and C termini of α 1C. *J Biol Chem* **275**, 39846–39854.

Jacquemond V (1997). Indo-1 fluorescence signals elicited by membrane depolarization in enzymatically isolated mouse skeletal muscle fibers. *Biophys J* **73**, 920–928.

Jean-Baptiste G, Yang Z, Khoury C, Gaudio S & Greenwood MT (2005). Peptide and non-peptide G-protein coupled receptors (GPCRs) in skeletal muscle. *Peptides* **26**, 1528–1536.

Johnson BD, Brousal JP, Peterson BZ, Gallombardo PA, Hockerman GH, Lai Y *et al.* (1997). Modulation of the cloned skeletal muscle L-type Ca^{2+} channel by anchored cAMP-dependent protein kinase. *J Neurosci* **17**, 1243–1255.

Lamb GD & Stephenson DG (1991). Excitation-contraction coupling in skeletal muscle fibres of rat and toad in the presence of GTPgS. *J Physiol* **444**, 65–84.

Legrand C, Giacomello E, Berthier C, Allard B, Sorrentino V & Jacquemond V (2008). Spontaneous and voltage-activated Ca^{2+} release in adult mouse skeletal muscle fibres expressing the type 3 ryanodine receptor. *J Physiol* **586**, 441–457.

Leong P & MacLennan DH (1998). The cytoplasmic loops between domains II and III and domains III and IV in the skeletal muscle dihydropyridine receptor bind to a contiguous site in the skeletal muscle ryanodine receptor. *J Biol Chem* **273**, 29958–29964.

Lu X, Xu L & Meissner G (1994). Activation of the skeletal muscle calcium release channel by a cytoplasmic loop of the dihydropyridine receptor. *J Biol Chem* **269**, 6511–6516.

McCudden CR, Hains MD, Kimple RJ, Siderovski DP & Willard FS (2005). G-protein signaling: back to the future. *Cell Mol Life Sci* **62**, 551–577.

Marchetti C, Carbone E & Lux HD (1986). Effects of dopamine and noradrenaline on Ca channels of cultured sensory and sympathetic neurons of chick. *Pflugers Arch* **406**, 104–111.

Milligan G & Kostenis E (2006). Heterotrimeric G-proteins: a short history. *Br J Pharmacol* **147**, S46–S55.

Pouvreau S & Jacquemond V (2005). Nitric oxide synthase inhibition affects sarcoplasmic reticulum Ca^{2+} release in skeletal muscle fibres from mouse. *J Physiol* **567**, 815–828.

Qin N, Platano D, Olcese R, Stefani E & Birnbaumer L (1997). Direct interaction of g$\beta\gamma$ with a C-terminal g$\beta\gamma$-binding domain of the Ca^{2+} channel α1 subunit is responsible for channel inhibition by G protein-coupled receptors. *Proc Natl Acad Sci USA* **94**, 8866–8871.

Scott RH & Dolphin AC (1990). Voltage-dependent modulation of rat sensory neurone calcium channel currents by G protein activation: effect of a dihydropyridine antagonist. *Br J Pharmacol* **99**, 629–630.

Sencer S, Papineni RV, Halling DB, Pate P, Krol J, Zhang JZ & Hamilton SL (2001). Coupling of RYR1 and L-type calcium channels via calmodulin binding domains. *J Biol Chem* **276**, 38237–38241.

Slavik KJ, Wang JP, Aghdasi B, Zhang JZ, Mandel F, Malouf N & Hamilton SL (1997). A carboxy-terminal peptide of the α1-subunit of the dihydropyridine receptor inhibits Ca^{2+}-release channels. *Am J Physiol Cell Physiol* **272**, C1475–C1481.

Somasundaram B, Tregear RT & Trentham DR (1991). GTPγS causes contraction of skinned frog skeletal muscle via the DHP-sensitive Ca^{2+} channels of sealed T-tubules. *Pflugers Arch* **418**, 137–143.

Strube C, Beurg M, Powers PA, Gregg RG & Coronado R (1996). Reduced Ca^{2+} current, charge movement, and absence of Ca^{2+} transients in skeletal muscle deficient in dihydropyridine receptor β1 subunit. *Biophys J* **71**, 2531–2543.

Tanabe T, Beam KG, Adams BA, Niidome T & Numa S (1990). Regions of the skeletal muscle dihydropyridine receptor critical for excitation-contraction coupling. *Nature* **346**, 567–569.

Tanaka H, Furuya T, Kameda N, Kobayashi T & Mizusawa H (2000). Triad proteins and intracellular Ca^{2+} transients during development of human skeletal muscle cells in aneural and innervated cultures. *J Muscle Res Cell Motil* **21**, 507–526.

Tedford HW & Zamponi GW (2006). Direct G protein modulation of Cav2 calcium channels. *Pharmacol Rev* **58**, 837–862.

Toutant M, Barhanin J, Bockaert J & Rouot B (1988). G-proteins in skeletal muscle. Evidence for a 40 kDa pertussis-toxin substrate in purified transverse tubules. *Biochem J* **254**, 405–409.

Toutant M, Gabrion J, Vandaele S, Peraldi-Roux S, Barhanin J, Bockaert J & Rouot B (1990). Cellular distribution and biochemical characterization of G proteins in skeletal muscle: comparative location with voltage-dependent calcium channels. *EMBO J* **9**, 363–369.

Villaz M, Robert M, Carrier L, Beeler T, Rouot B, Toutant M & Dupont Y (1989). G-protein dependent potentiation of calcium release from sarcoplasmic reticulum of skeletal muscle. *Cell Signal* **1**, 493–506.

Volpe P, Sandri C, Bortoloso E, Valle G & Nori A (2004). Topology of Homer 1c and Homer 1a in C2C12 myotubes and transgenic skeletal muscle fibers. *Biochem Biophys Res Commun* **316**, 884–892.

Weiss N, Couchoux H, Legrand C, Berthier C, Allard B & Jacquemond V (2008). Expression of the muscular dystrophy-associated caveolin-3(P104L) mutant in adult mouse skeletal muscle specifically alters the Ca^{2+} channel function of the dihydropyridine receptor. *Pflugers Arch* **457**, 361–375.

Weiss RG, O'Connell KM, Flucher BE, Allen PD, Grabner M & Dirksen RT (2004). Functional analysis of the R1086H malignant hyperthermia mutation in the DHPR reveals an unexpected influence of the III-IV loop on skeletal muscle EC coupling. *Am J Physiol Cell Physiol* **287**, C1094–C1102.

Wolfe JT, Wang H, Howard J, Garrison JC & Barrett PQ (2003). T-type calcium channel regulation by specific G-protein βg subunits. *Nature* **424**, 209–213.

Xiong Y, Zhou Y & Jarrett HW (2009). Dystrophin glycoprotein complex-associated G$\beta\gamma$ subunits activate phosphatidylinositol-3-kinase/Akt signaling in skeletal muscle in a laminin-dependent manner. *J Cell Physiol* **219**, 402–414.

Zamponi GW (2001). Determinants of G protein inhibition of presynaptic calcium channels. *Cell Biochem Biophys* **34**, 79–94.

Zamponi GW, Bourinet E, Nelson D, Nargeot J & Snutch TP (1997). Crosstalk between G proteins and protein kinase C mediated by the calcium channel α1 subunit. *Nature* **385**, 442–446.

Author contributions

N.W. and V.J. designed the study; N.W., C.L., S.P., H.B. and V.J. performed experiments; N.W. and V.J. analysed the data; N.W., B.A., G.W.Z., M.D.W. and V.J. wrote the paper. This study was conducted at the University Claude Bernard, Villeurbanne, France. All authors approved the final version of the manuscript.

Acknowledgements

This work was supported by grants from the Centre National de la Recherche Scientifique (CNRS), University Lyon 1 and the Canadian Institutes of Health Research. G.W.Z. is a Canada Research Chair and Scientist of the Alberta Heritage Foundation for Medical research.

Author's present address

N. Weiss: Grenoble Institut des Neurosciences – INSERM U836, Bât. Edmond J. Safra, chemin Fortuné Ferrini, Site santé La Tronche BP170, 38042 Grenoble Cedex 9, France.